Probing small-x gluons by low-mass Drell-Yan pairs at colliders

George Fai†, Jianwei Qiu‡, and Xiaofei Zhang†

† *CNR, Department of Physics, Kent State University, Kent, Ohio 44242, USA*

‡ *Department of Physics and Astronomy, Iowa State University, Ames, Iowa 50011, USA*

February 2, 2008

Abstract

The transverse-momentum (Q_T) distribution of low-mass Drell-Yan pairs is calculated in QCD perturbation theory with all-order resummation of $\alpha_s(\alpha_s \ln(Q_T^2/Q^2))^n$ type terms. We demonstrate that the rapidity distribution of low-mass Drell-Yan pairs at large-enough transverse momentum is an advantageous source of constraints on the gluon distribution and its nuclear dependence. We argue that low-mass Drell-Yan pairs in the forward region provide a good and clean probe of small-x gluons at collider energies.

12.38.Cy, 25.75.Dw

I. INTRODUCTION

Precise knowledge of the gluon distribution at small x is critical for reliable predictions of hard processes in hadron-hadron, hadron-nucleus, and nucleus-nucleus collisions at collider energies. Although tremendous effort has been invested in the study of the gluon distribution of a free hadron, there are still large uncertainties in the distribution in both the large and small x regions [1–4]. Because of the limited kinematic range that can be probed by fixed target arrangements, we have not had enough data to shed light on the gluon distribution in a nucleus. Thus, information on the gluon distribution in a nucleus is far from complete [5–16]. With better data from collider facilities, like the Relativistic Heavy Ion Collider (RHIC) and the future Large Hadron Collider (LHC), and also from the Tevatron at Fermilab, we expect much better information on the gluon distribution in free hadrons as well as in nuclei. In this paper, we demonstrate that the rapidity distribution of low-mass Drell-Yan pairs at large-enough transverse momentum is an advantageous source of constraints on the gluon distribution and its nuclear dependence.

A good process from the point of view of probing the gluon distribution must satisfy the following criteria: (i) it has to be reliably calculable within the factorization frame work of perturbative Quantum Chromodynamics (pQCD); (ii) its production cross section must be dominated by gluon-initiated sub-processes; and (iii) it should have sufficient production rate for the process to be observed. For probing the gluon distribution in a nucleus, we need to add another criterion: (iv) the process should have relatively small initial- and final-state medium effects because of the twist-2 nature of the gluon distribution.

It was first pointed out by Berger et al. [17] that the transverse-momentum distribution of Drell-Yan (massive) lepton pairs produced in hadronic collision is an advantageous source of constraints on the gluon distribution because of the dominance of gluon initiated subprocesses. These authors also emphasized that this process is free from the complications of photon isolation that beset studies of prompt photon production [17,18]. Due to the "Drell-Yan factor" in the cross section (the first factor on the right-hand side of Eq. (1) below),

it is useful to focus on low-mass Drell-Yan pairs to satisfy condition (iii). This, however, necessitates a recently-introduced resummation procedure [19].

In this paper we study the rapidity and transverse-momentum distribution of low-mass Drell-Yan pairs at RHIC, Tevatron and LHC energies, and the nuclear dependence of these distributions. (A short account of some aspects of the present work was given earlier [20].) In Sec. II the theoretical framework of our calculation is briefly reviewed. In Sec. III, we show that if the transverse momentum Q_T is larger than the invariant mass Q of the pair, the gluon initiated subprocesses give more than 80% of the low-mass Drell-Yan cross section at these colliders. We present our calculations for the cross sections of massive lepton-pair production at these collider energies in Sec. IV, and demonstrate that low-mass Drell-Yan lepton pairs are measurable. We also show that the gluon dominance does not reduce for all relevant rapidities. In Sec. V, we study the range of parton momentum fraction x that can be probed at these colliders while we vary the rapidities. We find that the forward region in rapidity is an excellent place to probe small-x gluons. In Sec. VI, we calculate the nuclear modification ratio, R_{AB}, for dAu, $AuAu$, pPb and $PbPb$ collisions. We investigate the effect of isospin for heavy ion beams, and the effect of nuclear modifications on parton distribution functions. We find that isospin plays an important role and study its impact on the R_{AB} ratio. We also observe an interesting dependence and constraint on the effective nuclear parton distributions. We point out that the forward suppression of Drell-Yan pair production in nucleus-nucleus collisions at LHC energies is expected to show a very different behavior from the pattern at RHIC. Our conclusions are given in Sec. VII.

II. CALCULATIONAL FRAMEWORK

The massive lepton pair of the Drell-Yan process is produced via the decay of an intermediate virtual photon, γ^*. Within the context of pQCD, the Drell-Yan cross section in a collision between hadrons A and B, $A(P_A) + B(P_B) \to \gamma^*(\to l\bar{l}(Q)) + X$, can be expressed in terms of the cross section for production of an unpolarized virtual photon of the same

invariant mass [17],

$$\frac{d\sigma_{AB\to\ell^+\ell^-(Q)X}}{dQ^2\,dQ_T^2\,dy} = \left(\frac{\alpha_{em}}{3\pi Q^2}\right)\frac{d\sigma_{AB\to\gamma^*(Q)X}}{dQ_T^2\,dy} \ , \tag{1}$$

with

$$\begin{aligned}\frac{d\sigma_{AB\to\gamma^*(Q)X}}{dQ_T^2\,dy} = &\sum_{a,b}\int dx_1\phi_{a/A}(x_1,\mu)\int dx_2\phi_{b/B}(x_2,\mu)\\ &\times\frac{d\hat{\sigma}_{ab\to\gamma^*(Q)X}}{dQ_T^2\,dy}(x_1,x_2,Q,Q_T,y;\mu) \ ,\end{aligned} \tag{2}$$

where $\Sigma_{a,b}$ runs over all parton flavors; the variables Q, Q_T, and y are the invariant mass, transverse momentum, and rapidity of the pair, respectively; X stands for an inclusive sum over final states that recoil against the virtual photon. In Eq. (2), the $\phi_{a/A}$ and $\phi_{b/B}$ are parton distribution functions, μ represents both the renormalization and the factorization scales (taken to be equal), and the $d\hat{\sigma}_{ab\to\gamma^*(Q)X}/dQ_T^2\,dy$ are short-distance hard parts calculated perturbatively order-by-order in powers of α_s. In Eq. (1), an integration has been performed over the angular distribution in the lepton-pair rest frame. Because of the Drell-Yan factor, $\alpha_{em}/(3\pi Q^2)$ in Eq. (1), the Drell-Yan cross section suffers from a low production rate [19].

To increase the production rate, it is desired to measure low-mass lepton pairs. On the other hand, the perturbatively calculated partonic hard parts, $d\hat{\sigma}_{ab\to\gamma^*(Q)X}/dQ_T^2\,dy$ in Eq. (2), have $\alpha_s(\alpha_s\ln(Q_T^2/Q^2))^n$ type large logarithms if $Q^2 \ll Q_T^2$, and the process has a potential of large background from open charm (or bottom) decay. Recently, it was shown [19] that the perturbatively factorized Drell-Yan cross section in Eq. (2) can be systematically re-organized into a new factorized form so that the $\alpha_s(\alpha_s\ln(Q_T^2/Q^2))^n$ type large logarithms are resummed to all orders in α_s:

$$\begin{aligned}\frac{d\sigma_{AB\to\gamma^*(Q)X}}{dQ_T^2\,dy} = &\sum_{a,b}\int dx_1\phi_{a/A}(x_1,\mu)\int dx_2\phi_{b/B}(x_2,\mu)\\ &\times\left\{\frac{d\hat{\sigma}^{(\mathrm{Dir})}_{ab\to\gamma^*(Q)X}}{dQ_T^2\,dy}(x_1,x_2,Q,Q_T,y;\mu_{\mathrm{Fr}},\mu)\right.\\ &+\sum_c\int\frac{dz}{z^2}\left[\frac{d\hat{\sigma}^{(\mathrm{F})}_{ab\to cX}}{dQ_{T_c}^2\,dy}(x_1,x_2,Q_c=\frac{\hat{Q}}{z};\mu_{\mathrm{Fr}},\mu)\right]\\ &\left.\times D_{c\to\gamma^*(Q)X}(z,\mu_{\mathrm{Fr}}^2;Q^2)\right\} \ ,\end{aligned} \tag{3}$$

where $\Sigma_{a,b}$ and Σ_c run over all parton flavors. In Eq. (3), $d\hat{\sigma}^{(\mathrm{Dir})}_{ab\to\gamma^*(Q)X}/dQ_T^2\,dy$ and $d\hat{\sigma}^{(\mathrm{F})}_{ab\to cX}/dQ_{T_c}^2\,dy$, are re-organized perturbatively calculated short-distance hard parts with the superscripts (Dir) and (F) indicating the direct and fragmentation contributions, respectively; the $D_{c\to\gamma^*(Q)X}$ are virtual photon fragmentation functions [21], which include all order resummation of the $\alpha_s(\alpha_s\ln(Q_T^2/Q^2))^n$ type large logarithms. The quantity μ_{Fr} represents the fragmentation scale. The four-vector $\hat{Q}^\mu$ is defined to be Q^μ but with Q^2 set to be zero. The CTEQ5M parton distribution functions (PDFs) are used in our calculations reported here, with all scales set to $\sqrt{Q_T^2+Q^2}$. This combination of the physical scales in the problem appears very natural and has appropriate limits when $Q_T^2 \ll Q^2$ and when $Q^2 \ll Q_T^2$. We are primarily interested in the latter case in the present work.

As pointed out in Ref. [19], the resummation of the $\alpha_s(\alpha_s\ln(Q_T^2/Q^2))^n$ type large logarithms is to re-organize the perturbative short-distance hard part, $d\hat{\sigma}_{ab\to\gamma^*(Q)X}/dQ_T^2\,dy$ in Eq. (2) into a "direct", $d\hat{\sigma}^{(\mathrm{Dir})}_{ab\to\gamma^*(Q)X}/dQ_T^2\,dy$, and a "fragmentation" contribution, $d\hat{\sigma}^{(\mathrm{F})}_{ab\to cX}/dp_{T_c}^2\,dy$, (Eq. (3)). It is important to realize that the direct and fragmentation contributions each have their separate perturbative expansions, recasting the single expansion of the conventional QCD factorization approach into two series [19]. A significant advantage of this re-organization is that the direct and fragmentation expansions are evaluated at a single hard scale and are free of large logarithms, and consequently, much more stable perturbatively.

III. GLUON-INITIATED CONTRIBUTION

To study the relative size of gluon-initiated contributions, we define the ratio

$$R_g = \frac{d\sigma_{AB\to\gamma^*(Q)X}(\text{gluon-initiated})}{dQ_T^2\,dy} \Big/ \frac{d\sigma_{AB\to\gamma^*(Q)X}}{dQ_T^2\,dy} \quad . \tag{4}$$

The numerator includes the contributions from all partonic sub-processes with at least one initial-state gluon, and the denominator includes all sub-processes. In Fig. 1(a), we show R_g as a function of Q_T at fixed y, while Fig. 1(b) displays R_g as a function of y at fixed Q_T at $Q = 2$ GeV for proton-proton collision at RHIC energy.

FIGURES

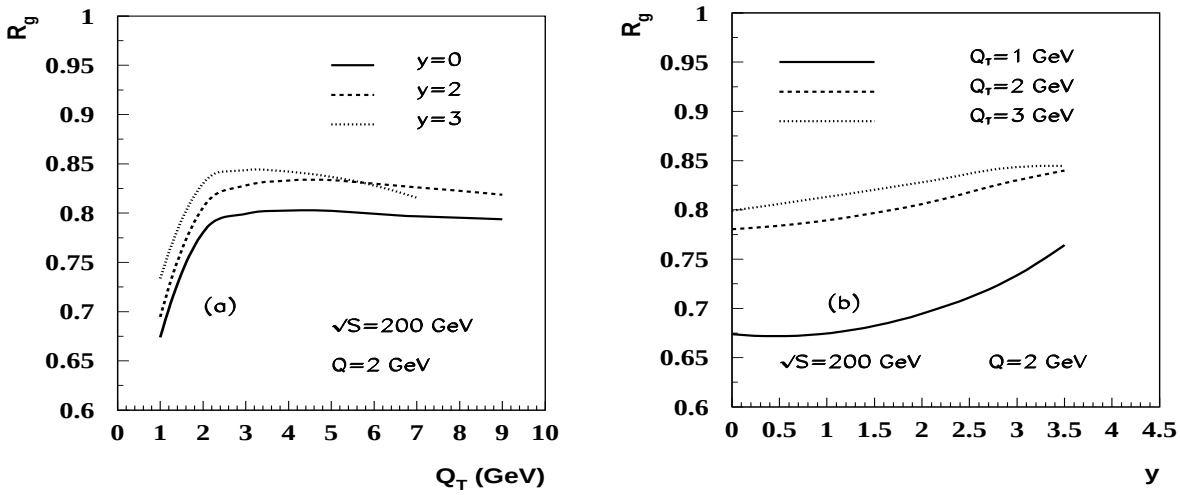

FIG. 1. The ratio R_g defined in Eq. (4) with $Q = 2$ GeV at $\sqrt{s} = 200$ GeV. Part (a): R_g as a function of Q_T for different rapidities; part (b): R_g as a function of rapidity y for different transverse momenta.

Figures 2 and 3 contain similar information for proton-antiproton collision at Tevatron energies, $\sqrt{s} = 630$ GeV and $\sqrt{s} = 1960$ GeV, respectively.

The Q_T dependence of R_g shows a rapid increase up to $Q_T \approx Q$, followed by a plateau with a value at around (or above) 0.8 at all energies. This confirms that, for sufficiently large Q_T, gluon-initiated sub-processes dominate the Drell-Yan cross section and thus low-mass Drell-Yan lepton-pair production at large transverse momentum is an excellent source of information on the gluon distribution at RHIC, Tevatron and LHC energies [17]. The fall-off of R_g towards very large Q_T is related to the reduction of phase space and to the fact that the cross sections are evaluated at larger values of the parton momentum fractions. As a function of rapidity, R_g increases slightly as one moves in the forward direction (in particular at RHIC energy, see parts (b) of the Figures). This already calls attention to the forward region as a good kinematical domain to test gluon distributions. An example of the energy dependence of R_g is displayed in Fig. 4. We see that R_g increases slightly as $\sqrt{s}$ increases, but the dependence is not too strong. (Note the logarithmic scale for $\sqrt{s}$.)

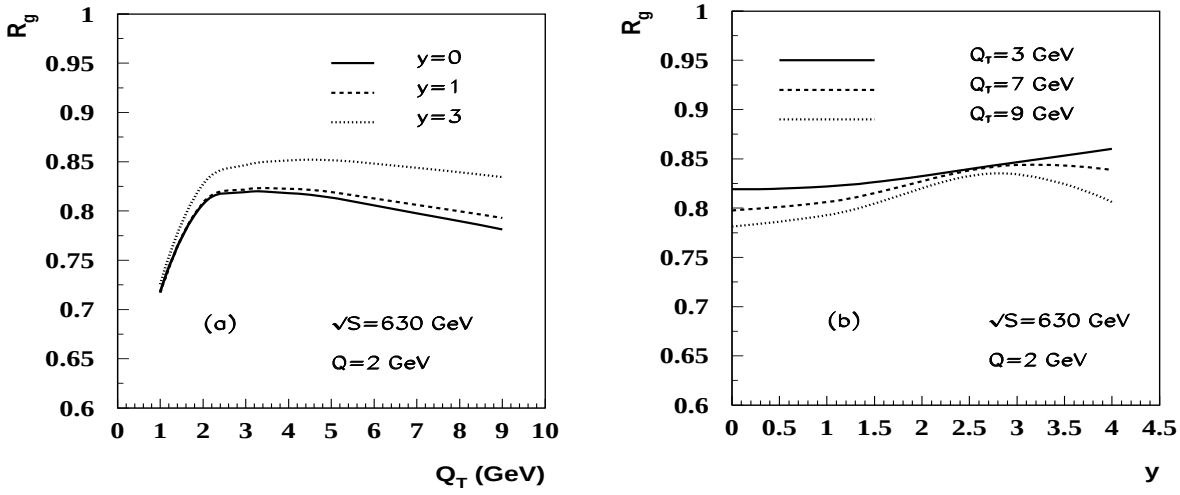

FIG. 2. The ratio R_g defined in Eq. (4) with $Q = 2$ GeV at $\sqrt{s} = 630$ GeV. Part (a): R_g as a function of Q_T for different rapidities; part (b): R_g as a function of rapidity y for different transverse momenta.

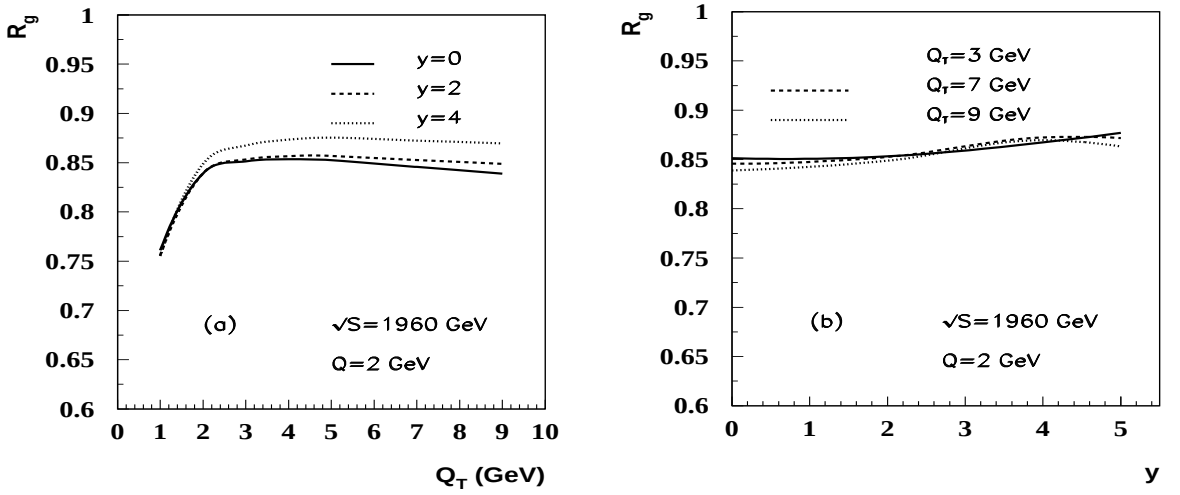

FIG. 3. The ratio R_g defined in Eq. (4) with $Q = 2$ GeV at $\sqrt{s} = 1.96$ TeV. Part (a): R_g as a function of Q_T for different rapidities; part (b): R_g as a function of rapidity y for different transverse momenta.

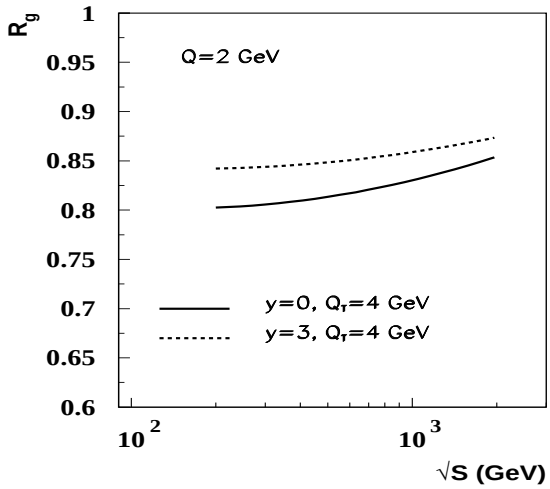

FIG. 4. The c.m. energy dependence of the ratio R_g defined in Eq. (4) for Q =2 GeV, Q_T = 4 GeV, $y = 0$ (solid) and $y = 3$ (dashed). Note the logarithmic energy scale.

IV. THE DRELL-YAN CROSS SECTION AT RHIC AND TEVATRON ENERGIES

Recalling criterion (iii) in the Introduction, we now turn to the production rate of low-mass Drell-Yan pairs at RHIC and Tevatron. We present the Drell-Yan cross section at large transverse momentum with all-order resummation. For Drell-Yan pair production, as seen from Eq. (1), there is a phase space penalty associated with the finite mass of the virtual photon, and the Drell-Yan factor, $\alpha_{em}/(3\pi Q^2) < 10^{-3}/Q^2$, renders the production rate for massive lepton pairs small at large values of Q. In addition, the spectra drop rapidly with increasing Q_T. In order to enhance the Drell-Yan cross section while keeping the dominance of the gluon initiated sub-processes, it is useful to study lepton pairs with low invariant mass and relatively large transverse momentum [19]. With the large transverse momentum Q_T setting the hard scale of the collision, the invariant mass of the virtual photon Q can be small, as long as the process can be identified experimentally, and $Q \gg \Lambda_{\rm QCD}$. For example, the cross section for Drell-Yan production was measured by the CERN UA1 Collaboration [22] for virtual photon mass $Q \in [2m_\mu, 2.5]$ GeV.

Figure 5 shows the all-order resummed result for the Drell-Yan cross section as a function of Q_T at the RHIC energy of $\sqrt{s} = 200$ GeV and rapidity $y = 0$ for two values of the mass,

(a) $Q = 1$ GeV and (b) $Q = 2$ GeV. The cross section increases by about a factor 10 when the Drell-Yan mass decreases from 2 GeV to 1 GeV. It might still be a challenge to measure the low-mass Drell-Yan production with the production rate shown in Fig. 5. At the LHC, both the collision energy and luminosity are significantly improved. Our calculation shows that the production rate at the LHC is sufficiently large for being measured. (We also calculated R_g for $Q = 1$ GeV. When Q decreases to 1 GeV, we find that R_g actually increases slightly in the $Q_T \sim 1$ GeV region and it is similar to the $Q = 2$ GeV case in the high Q_T region.)

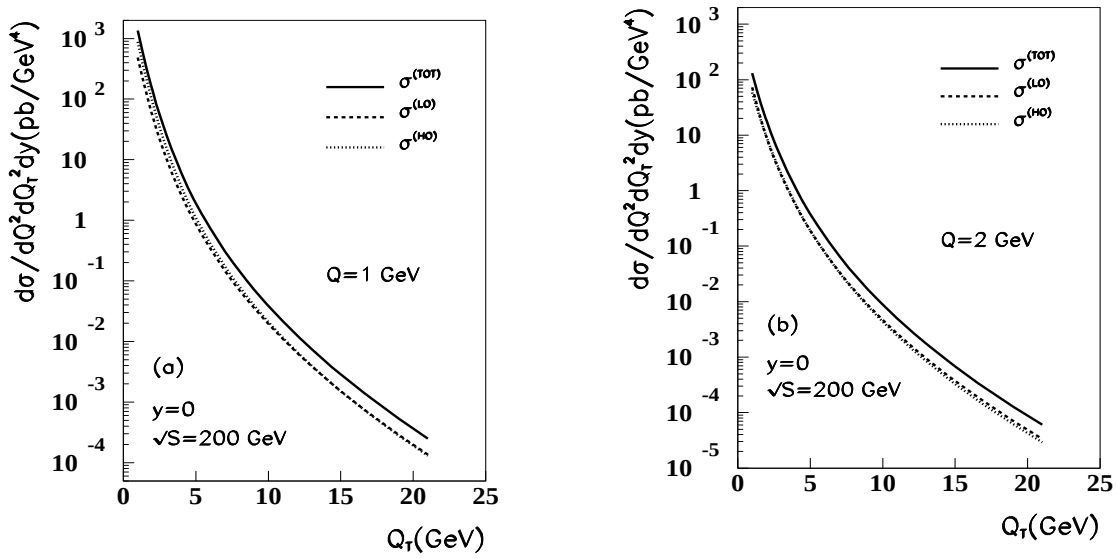

FIG. 5. Drell-Yan cross section as a function of Q_T at RHIC energy $\sqrt{s} = 200$ GeV and rapidity $y = 0$, for (a) mass $Q = 1$ GeV, and (b) $Q = 2$ GeV. The top (solid) lines represent the total cross sections; leading-order (LO, dashed) and higher-order (HO, dotted) contributions are also shown.

Figure 6 displays similar results for the Tevatron energies of $\sqrt{s} = 1.96$ TeV ((a) and (b)) and $\sqrt{s} = 630$ GeV (c). For the larger energy, we show results with (a) $Q = 5$ GeV and (b) $Q = 2$ GeV. The cross section is about 20 times larger for $Q = 2$ GeV than for $Q = 5$ GeV at any fixed Q_T.

In Figs. 5 and 6 we separately show the leading-order (LO, dashed), and higher-order (HO, dotted) contributions. At high Q_T the LO and HO contributions are roughly comparable. The total cross section can also be broken up into gluon-initiated, quark-quark, and

resummed contributions. Results on this composition are published elsewhere [20].

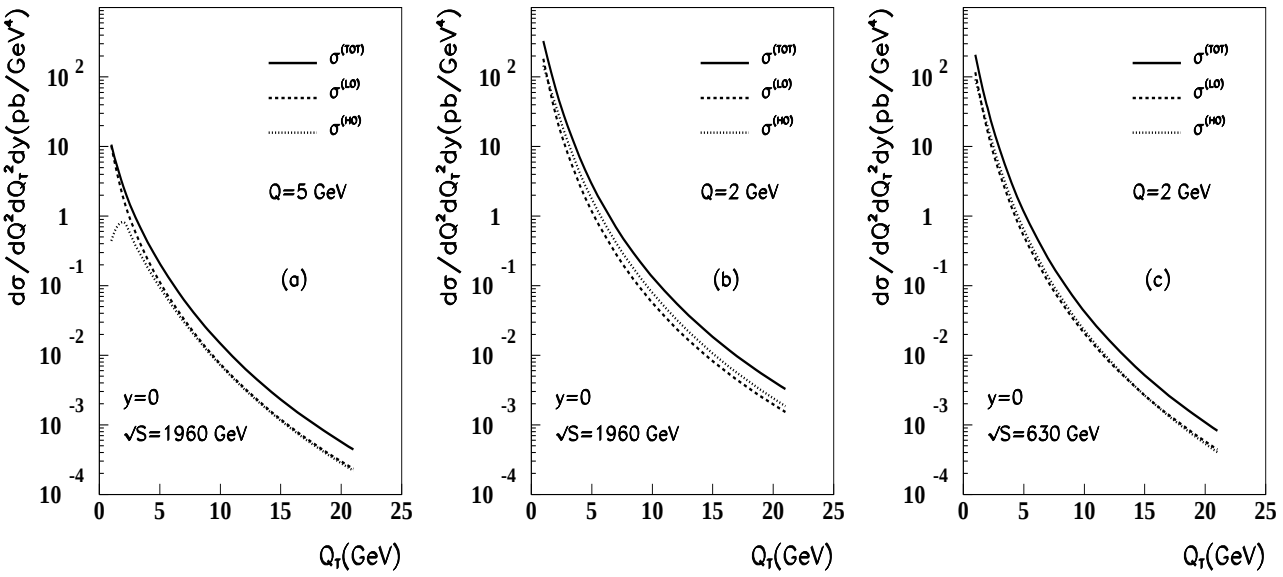

FIG. 6. Drell-Yan cross section at rapidity $y = 0$ as a function of Q_T at Tevatron energies: (a) $\sqrt{s} = 1.96$ TeV and $Q = 5$ GeV; (b) $\sqrt{s} = 1.96$ TeV and $Q = 2$ GeV; and (c) $\sqrt{s} = 630$ GeV and $Q = 2$ GeV. The top (solid) lines represent the total cross sections; leading-order (LO, dashed) and higher-order (HO, dotted) contributions are also shown.

Figures 7 and 8 present the rapidity dependence of the cross sections at RHIC and Tevatron energies at various values of Q and Q_T. It can be seen that while there are order-of-magnitude differences in the cross section between different values of Q and Q_T, the rapidity distributions remain flat upto high absolute values of y. This lends further support to the idea of exploring forward rapidities. As we will see in Section V, the forward region is an excellent place to probe small-x gluons.

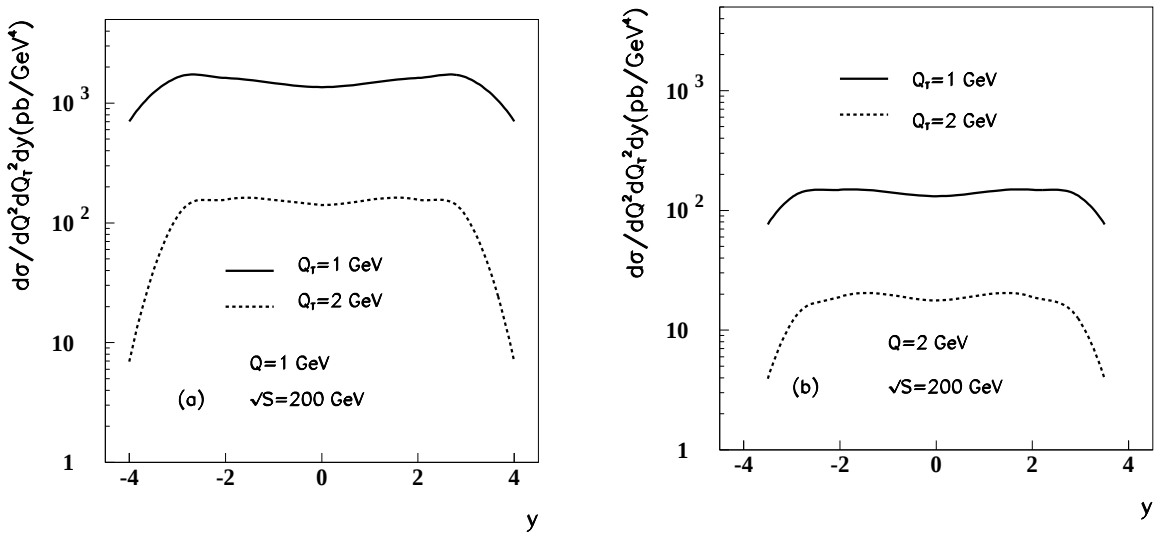

FIG. 7. Drell-Yan cross section as a function of y at RHIC energy $\sqrt{s} = 200$ GeV with $Q_T = 1$ GeV (solid) and $Q_T = 2$ GeV (dashed) for (a) $Q = 1$ GeV and (b) $Q = 2$ GeV.

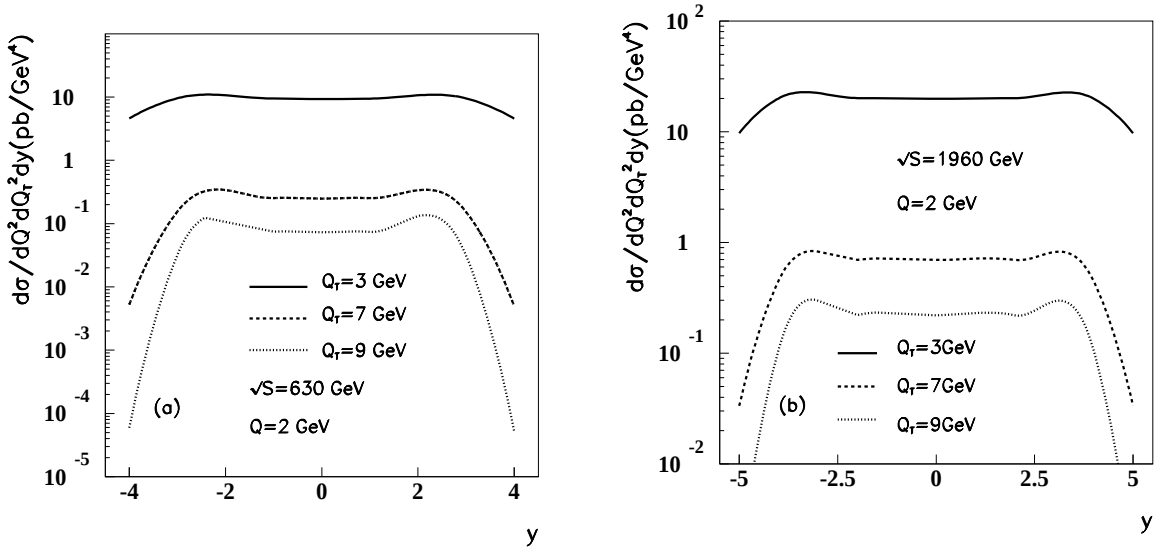

FIG. 8. Drell-Yan cross section as a function of rapidity y for $Q = 2$ GeV and $Q_T = 3$ GeV (solid), 7 GeV (dashed), and 9 GeV (dotted) at Tevatron energies: (a) $\sqrt{s} = 630$ GeV, and (b) $\sqrt{s} = 1960$ GeV.

V. PARTON MOMENTUM FRACTION PROBED

It is very important to estimate the region of x in the gluon distribution probed by the low-mass Drell-Yan process. Let us use x_1 to refer to partons in one of the beams (say the "yellow" beam in the RHIC color code), and x_2 for partons in the other ("blue") beam. The x_1 and x_2 integrations of the Dell-Yan cross section run from the appropriate minimum values (given by the kinematics) to 1. At central rapidity $y = 0$, the integration is symmetric in x_1 and x_2. We are most interested in small x physics. We expect a large fraction of the cross section to come from rather small values of x_2 in the forward region from the perspective of the yellow beam, where x_1 is not small. To quantify our statement with respect to x_2, we introduce a cutoff x_{cut} to limit the x_2 integration to the interval x_{min} to x_{cut} for partons in the blue beam. Let us define the ratio

$$R_{x_2} = \int_{x_{\rm min}}^{x_{\rm cut}} dx_2 \left(\frac{d\sigma^{\rm DY}}{dx_2}\right) \Big/ \int_{x_{\rm min}}^{1} dx_2 \left(\frac{d\sigma^{\rm DY}}{dx_2}\right) \quad . \tag{5}$$

Due to the symmetry in x_1 and x_2, at central rapidities it is enough to examine the shape of R_{x_2} to establish which region dominates the x integration — the region of x low-mass Drell-Yan data can provide precise information about. In Fig. 9(a) we plot R_{x_2} at RHIC, as a function of x_{cut} for $Q = 1$ GeV for different rapidities and transverse momenta. Figure 9(a) shows that in the central rapidity region $x_2 \sim [10^{-2}, 10^{-1}]$ dominates the integration for both $Q_T = 1$ GeV and $Q_T = 3$ GeV when $y = 0$ at RHIC.

Figure 9(a) also provides important information about the forward region (from the perspective of x_1). At $y = 3$, 90% of the cross-section is given by $x_2 < 0.01$, which is exactly the shadowing region of the nuclear parton distribution function. This region dominates the integration for both $Q_T = 1$ GeV and $Q_T = 3$ GeV when $y = 3$. Our calculation for the rapidity distribution of the total cross section (see Fig. 7) shows that the cross section does not start to drop until $y \sim 3$. In other words, the production rate in the large-rapidity region is not significantly smaller than in the central region, as long as $|y| \leq 3$. While, as indicated by Fig. 9(a), the typical x_2 is much smaller in the forward region than at $y = 0$,

the situation is different for x_1. In order to evaluate the important region of x_1 for Drell-Yan production, we define the analogous ratio (compare to Eq. (5))

$$R_{x_1} = \int_{x_{\rm min}}^{x_{\rm cut}} dx_1 \left(\frac{d\sigma^{\rm DY}}{dx_1}\right) \Big/ \int_{x_{\rm min}}^{1} dx_1 \left(\frac{d\sigma^{\rm DY}}{dx_1}\right) \quad . \tag{6}$$

In Fig. 9(b), we plot R_{x_1} for forward rapidity $y = 3$ and Q =1 GeV at $Q_T = 1$ GeV (solid) and $Q_T = 3$ GeV (dashed). For $Q_T = 1$ GeV, the dominant region is $x_1 \sim [0.1, 0.3]$ and for $Q_T = 3$ GeV, the dominant region is $x_1 \sim [0.3, 0.7]$. (The ratio R_{x_1} for $y = 0$ is of course identical to R_{x_2} for $y = 0$ due to the symmetry, and thus can be seen in Fig. 9(a).) As we will discuss later, the dominant x_2 region plays an important role in the nuclear effects on Drell-Yan production in an AB nuclear collision.

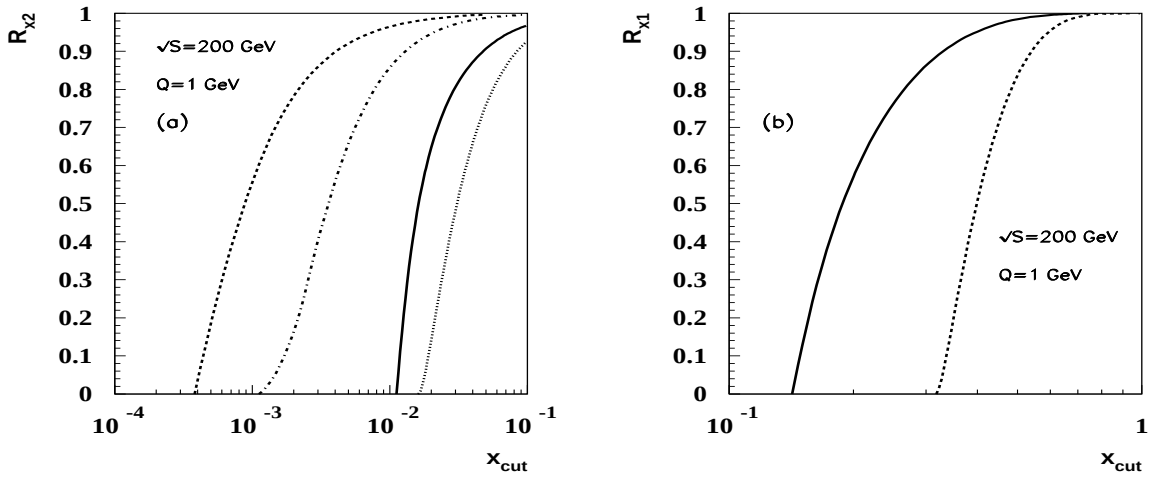

FIG. 9. The ratios R_{x2} (defined in Eq. (5)) and R_{x1} (Eq. (6)) for $Q = 1$ GeV at RHIC energy, $\sqrt{s} = 200$ GeV. In (a), both central rapidities: $y = 0, Q_T = 1$ GeV (solid); $y = 0, Q_T = 3$ GeV (dotted), and forward rapidities: $y = 3, Q_T = 1$ GeV (dashed); $y = 3, Q_T = 3$ GeV (dot-dashed) are shown. In (b) R_{x1} is displayed at forward rapidities: $y = 3, Q_T = 1$ GeV (solid); $y = 3, Q_T = 3$ GeV (dashed). See text for more explanation.

Figures 10 and 11 are similar to Fig. 9, but for the top Tevatron energy of $\sqrt{s}$ =1.96 TeV and for the LHC energy of 5.5 TeV, respectively. Fig. 10(a) displays R_{x_2} as a function of x_{cut} for $Q = 2$ GeV for different rapidities and transverse momenta Q_T. Fig. 10(b) shows R_{x_1} for $y = 3$ at $Q_T = 3$ GeV and $Q_T = 7$ GeV. It can be seen from Fig. 10(a) that the

dominant region in x_2 at central rapidity is $x_2 \sim [10^{-3}, 10^{-2}]$ at the top Tevatron energy; at forward rapidities $x_2 < 10^{-4}$ is reached. For x_1 in the forward region, the dominant contribution comes from $x_1 \sim [4 * 10^{-2}, 10^{-1}]$, as seen in Fig. 10(b). In Fig. 11(a) we plot R_{x_2} as a function of x_{cut} for $Q = 2$ GeV for different rapidities and transverse momenta at the LHC. Figure 11(a) shows that in the central rapidity region, even when $Q_T = 10$ GeV, $x_2 < 0.01$, i.e. the shadowing region, dominates the contribution to the Drell-Yan cross section. In the forward rapidity region with $y = 2.4$, low-mass Drell-Yan production will probe partons with x_2 as small as on the order of 10^{-5}. In Fig. 11(b), we plot R_{x_1} for $y = 2.4$ at $Q_T = 2$ GeV and $Q_T = 10$ GeV. The information provided here will be used in the next section (Section VI) to discuss the nuclear effects in the forward region at the LHC.

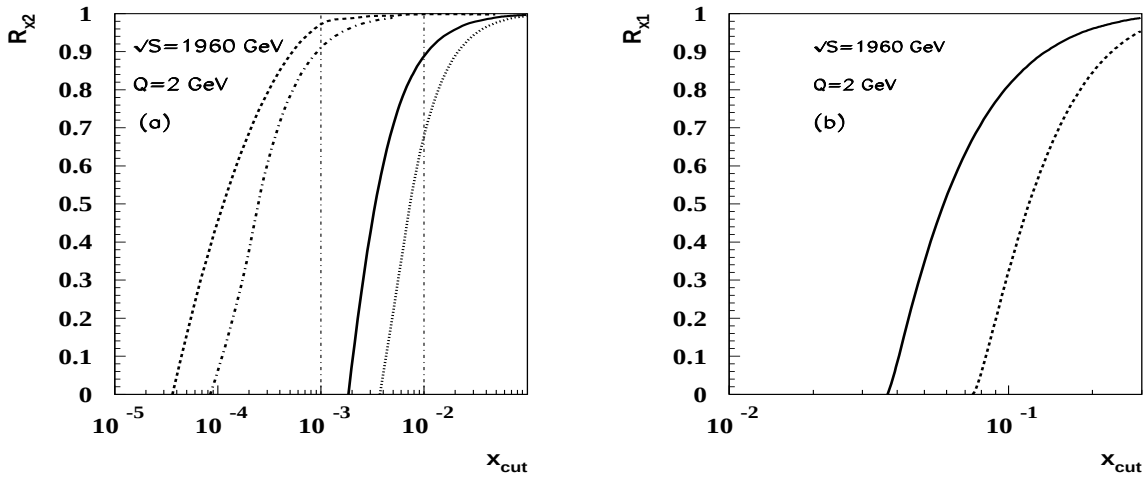

FIG. 10. The ratios R_{x2} (defined in Eq. (5)) and R_{x1} (Eq. (6)) for $Q = 2$ GeV at Tevatron energy, $\sqrt{s} = 1.96$ TeV. In (a), both central rapidities: $y = 0, Q_T = 3$ GeV (solid); $y = 0, Q_T = 7$ GeV (dotted), and forward rapidities: $y = 3, Q_T = 3$ GeV (dashed); $y = 3, Q_T = 7$ GeV (dot-dashed) are shown. In (b) R_{x1} is displayed at forward rapidities: $y = 3, Q_T = 3$ GeV (solid); $y = 3, Q_T = 7$ GeV (dashed).

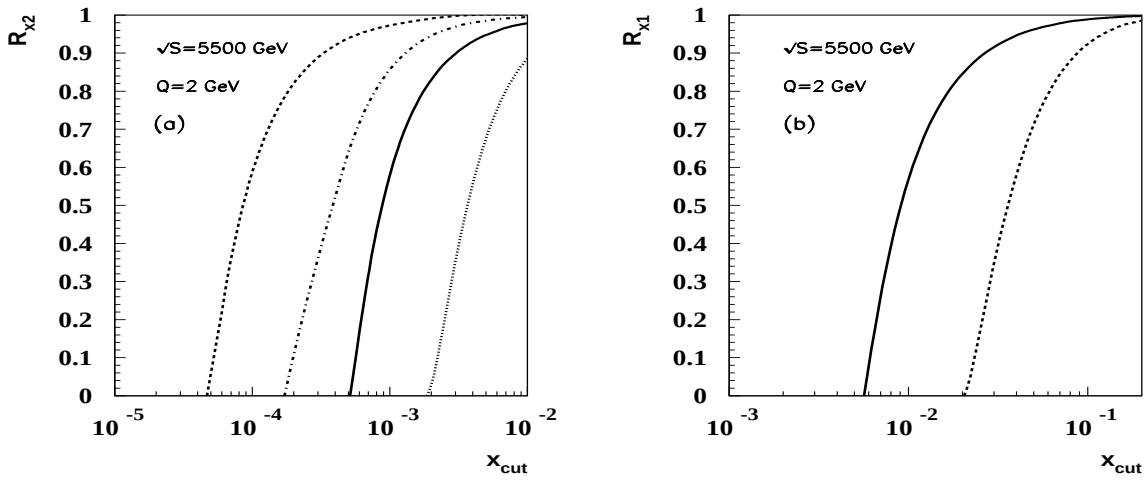

FIG. 11. The ratios (a) R_{x_2} and (b) R_{x_1} for $Q = 2$ GeV at LHC $\sqrt{s} = 5500$ GeV. Different lines in (a) represent R_{x2} at different y and Q_T: $y = 0, Q_T = 2$ GeV (solid); $y = 0, Q_T = 10$ GeV (dotted); $y = 2.4, Q_T = 2$ GeV (dashed); $y = 2.4, Q_T = 10$ GeV (dot-dashed). In (b) we have $y = 2.4, Q_T = 2$ GeV (solid) and $y = 2.4, Q_T = 10$ GeV (dashed).

VI. NUCLEAR EFFECTS AT RHIC AND LHC

In lack of nuclear effects on the hard collision, the impact-parameter integrated production cross section of low-mass Drell-Yan pairs in nucleus-nucleus (AB) collisions should scale, compared to the production in pp collisions, as the number of binary collisions. However, there are several nuclear effects on the hard collision in a heavy-ion reaction. For high transverse-momentum Drell-Yan production, two kinds of nuclear effects are expected to play an important role: isospin effects and the modification of the parton distribution function in the nucleus (shadowing effect). In this Section, we calculate a "nuclear modification factor" R_{AB} at RHIC and LHC, and discuss isospin and shadowing effects in Drell-Yan production. We consider different rapidities, and for the RHIC program, compare $AuAu$ and dAu collisions. Isospin effects were recently also emphasized in dAu scattering at forward rapidities in Ref. [23].

Similarly to the "nuclear modification factor" in hadron production, we define a ratio,

$$R_{AB}(Q_T) \equiv \frac{d\sigma^{(sh)}(Z_A/A, Z_B/B)}{dQ_T^2 dy} \Big/ \frac{d\sigma}{dQ_T^2 dy} \ , \tag{7}$$

where Z_A and Z_B are the atomic numbers and A and B are the mass numbers of the colliding nuclei, and the cross section $d\sigma^{(sh)}(Z_A/A, Z_B/B)/dQ_T^2 dy$ uses nuclear PDFs defined in Eq. (8) below, while $d\sigma/dQ_T^2 dy$ is the pp cross section defined in Eq. (2). Thus, R_{AB} incorporates the effects of both shadowing and nuclear composition (isospin effect).

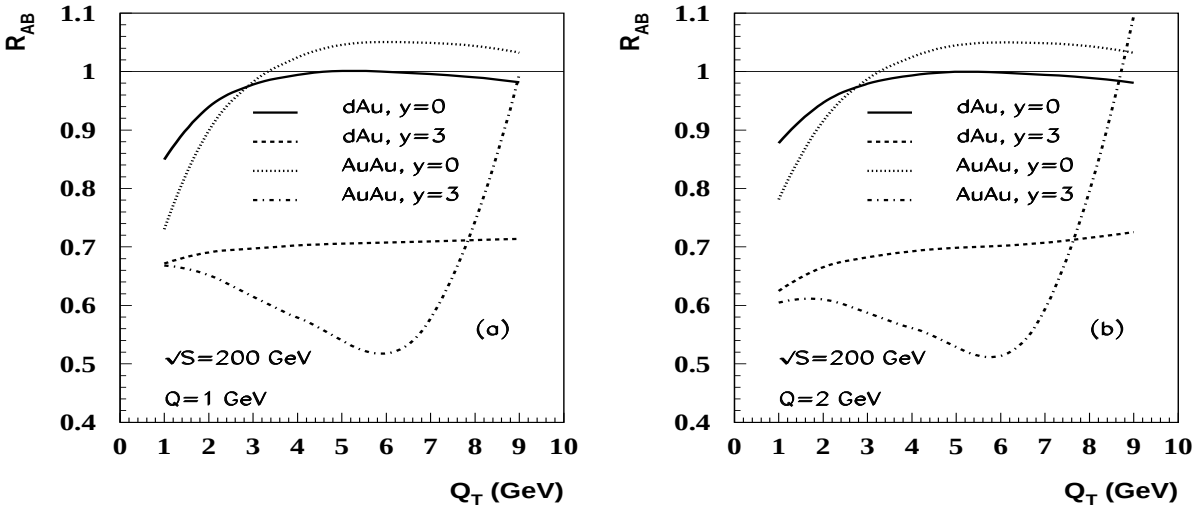

FIG. 12. The ratio R_{AB} defined in Eq. (7) for (a) $Q = 1$ GeV and (b) $Q = 2$ GeV. Different lines in the figure represent R_{AB} at different values of y for different collisions.

In Fig. 12, we plot R_{AB} as a function of Q_T at RHIC in dAu and $AuAu$ collisions at both central rapidity ($y = 0$) and forward rapidity ($y = 3$) for (a) $Q = 1$ GeV and (b) $Q = 2$ GeV. In this work we use the EKS parameterization to incorporate the shadowing effect in the nuclear PDF [8]. Numerical differences from using other nuclear PDF parameterizations [5,10–13,15] could be estimated from the ranges of momentum fraction x probed at different collision energies. Fig. 12 shows that in the central rapidity region, R_{dAu} is larger than R_{AuAu} in the small Q_T region, and R_{AuAu} becomes larger than one and larger than R_{dAu} when Q_T is larger than ≈ 3 GeV. This seems to be surprising at first glance. Fig. 12 also shows strong suppression of Drell-Yan pair production in both dAu and $AuAu$ collisions in the forward region. Furthermore, R_{AuAu} increases steeply at large $Q_T > 6$ GeV when $y = 3$. In order to

disentangle shadowing and isospin effects, both incorporated in R_{AB} as defined in Eq.(7), we separate these dependences and investigate isospin and shadowing effects separately in the following discussion.

To take into account the neutron-proton composition of nuclei one normally uses

$$\Phi_{a/A} = \frac{Z_A}{A}\Phi^p_{a/A} + (1 - \frac{Z_A}{A})\Phi^n_{a/A} \tag{8}$$

for the nuclear PDF, where $\Phi^p_{a/A}$ is the proton PDF and $\Phi^n_{a/A}$ is the PDF of the neutron. By artificially setting $Z_A = A$ and $Z_B = B$ in our calculation, we consider nuclei made of protons only. Calculating the analogue of (7) for these hypothetical nuclei we define R^{sh}_{AB}, which is free of isospin effects and contains shadowing only (pure shadowing). The ratio R^{sh}_{AB} is shown at $y = 0$ in Fig. 13 by the dotted lines for (a) dAu and (b) $AuAu$ collisions.

It can be seen from Fig. 13 that in the central rapidity region, when $Q_T > 3$ GeV, R^{sh}_{AB} is larger than 1 in both $AuAu$ and dAu collisions. This means that anti-shadowing in the PDF start to be important at $Q_T \sim 3$ GeV. The result is consistent with what was learned about the dominant region of x earlier. Recall from Fig. 9(a) that the dominant region of x for partons from both beams is about $[10^{-2}, 10^{-1}]$ for $Q_T = 3$ GeV and $y = 0$. An inspection of the EKS nuclear PDFs [8] informs that $x \sim 10^{-1}$ is the region where anti-shadowing starts to take over shadowing. In $AuAu$ collisions, partons in both beams experience the same shadowing (anti-shadowing) effects at central rapidity. In dAu collisions, only the partons in the Au nucleus have significant shadowing (anti-shadowing) effects. Therefore pure shadowing (anti-shadowing) effects are stronger in the $AuAu$ collisions than in the dAu collisions as seen in Fig. 13.

Now let us also investigate the pure isospin effects on low-mass Drell-Yan production. Isospin effects originate in the difference between the parton distributions of neutrons and protons. Due to this difference, the production cross section of Drell-Yan pairs in proton-neutron and neutron-neutron interactions differs from that in pp collisions. To study isospin effects, let us introduce

$$R^{iso}_{AB}(Q_T) \equiv \frac{d\sigma(Z_A/A, Z_B/B)}{dQ^2_T dy} \Big/ \frac{d\sigma}{dQ^2_T dy} \ , \tag{9}$$

where the numerator now does not include shadowing, i.e. standard CTEQ5M PDFs are used without shadowing. Examining R_{AB}^{iso} completes our program of separating the isospin and shadowing dependences of Eq. (7).

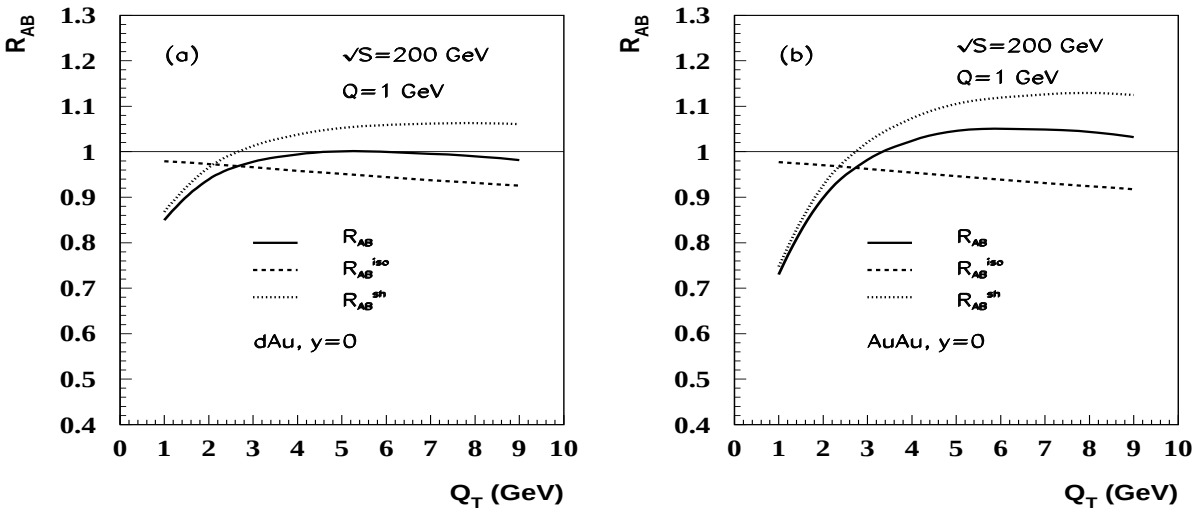

FIG. 13. The pure shadowing (dotted) and isospin (dashed) components of ratio R_{AB} at $y = 0$ and Q =1 GeV at RHIC for (a) dAu and (b) $AuAu$ collisions. See text for more explanation.

Figure 13 also displays R_{AB}^{iso} (dashed line) as a function of Q_T in (a) dAu and (b) $AuAu$ collisions at $y = 0$. We see that $R_{AB}^{iso} < 1$ in the whole transverse momentum region $[1, 10]$ GeV; isospin effects suppress the production of high transverse-momentum low-mass Drell-Yan pairs at RHIC. The suppression is getting slightly stronger with increasing Q_T. Since the Compton type (qg) processes are the dominant sub-processes in low-mass Drell-Yan production at high transverse momentum, we next consider the isospin effects in these sub-processes to help us understand the suppression result shown in Fig. 13. The contribution of different flavor quarks is proportional to the square of their fractional charges (charge factors): 4/9 for u quarks and 1/9 for d quarks. Let us first look at proton-proton (pp) and proton-neutron (pn) collisions. In the calculation of the pp Drell-Yan production cross section, the PDF part for the Compton-type processes, after including the charge factors, is proportional to $\Phi_g(4\Phi_u/9 + \Phi_d/9 + 4\Phi_{\bar{u}}/9 + \Phi_{\bar{d}}/9 + \cdots)$, plus an "exchange" term, where the gluon comes from the other proton. For pn, when the gluon comes from the proton, we have

$\Phi_g(\Phi_u/9+4\Phi_d/9+\Phi_{\bar{u}}/9+4\Phi_{\bar{d}}/9+\cdots)$ (where $\cdots$ represents the contributions which are the same for pp and pn), plus an exchange term. In Fig. 14, we plot $\Phi_d(x,\mu)/\Phi_u(x,\mu)$ (solid), $\Phi_{\bar{d}}(x,\mu)/\Phi_{\bar{u}}(x,\mu)$ (dashed), and the ratio of the above two charge-weighted expressions (dotted) as functions of x at the scale $\mu^2 = 10$ GeV^2. For not-too-small x, in particular in the region of $[10^{-2}, 10^{-1}]$, which is the dominant region of parton x, valence quarks are more important than sea quarks. Since $\Phi_d(x,\mu)/\Phi_u(x,\mu)$ (solid) is itself smaller than one, the production cross section in pn is smaller than in pp collisions. The dotted line in Fig. 14 illustrates the effect. Using a similar argument, one finds that the isospin effect in nn collisions is a little stronger than in pn collisions. Returning to nuclear reactions, where a large fraction of the nucleon-nucleon collisions is not pp, but pn and nn, we conclude that due to the charge factor and the fact that $\Phi_d < \Phi_u$ in the x region of interest, R_{AB}^{iso} is smaller than 1. When the transverse momentum increases, x in the PDFs increases. Since the ratio of Φ_d/Φ_u becomes smaller at larger x, R_{AB}^{iso} decreases as Q_T increases. Since the change of the proton/neutron ratio from d to Au is small for these purposes, R_{AB}^{iso} is very similar in dAu to that of $AuAu$, as Fig. 13 demonstrates.

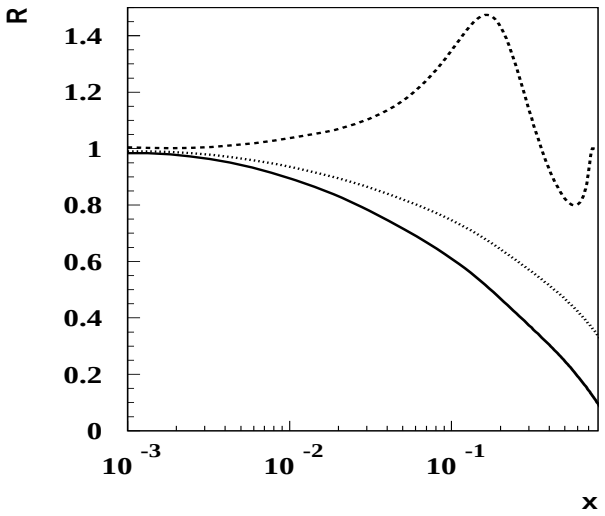

FIG. 14. The ratio of the d quark and u quark PDF-s and the charge-weighted ratio at scale Q^2 =10 GeV^2. See text for more explanation.

To summarize the above discussion, at central rapidity $y = 0$, when $Q_T > 3$ GeV, low-mass Drell-Yan pair production at RHIC suffers anti-shadowing. The anti-shadowing effects are stronger in $AuAu$ collisions than in dAu collisions; isospin effects suppress the production of low-mass Drell-Yan pairs and the suppression increase with Q_T; isospin effects are similar in dAu and $AuAu$ collisions. The combined effects of isospin and shadowing lead to a larger R_{AB} in $AuAu$ than in dAu at RHIC energy.

Figure 15 displays results for R_{AB} (solid), R_{AB}^{iso} (dashed), and R_{AB}^{sh} (dotted) in the forward region for (a) dAu and (b) $AuAu$ collisions. It is clear that the steep rise of R_{AB} at large transverse momentum in $AuAu$ collisions is a consequence of the effects of the modification of the nuclear PDF in the "yellow" beam (for which $y = 3$ designates the forward region); correspondingly x_1 enters the Fermi-motion region of the nuclear PDF. The large suppression due to isospin effects, which reaches $\approx 40\%$ at high transverse momentum is also from the "yellow" beam side, where the larger x_1 gives a stronger u, d asymmetry. To demonstrate this point, we also plot R_{pAu} in Fig. 15(a) (dot-dashed). The result $R_{pAu} \sim 1$ confirms that the large isospin effect in dAu is from the d side. It is also important to point out the big difference between R_{pAu} and R_{dAu}, which illustrates that, in regard to certain observables, dAu collisions can be very different from pA collisions.

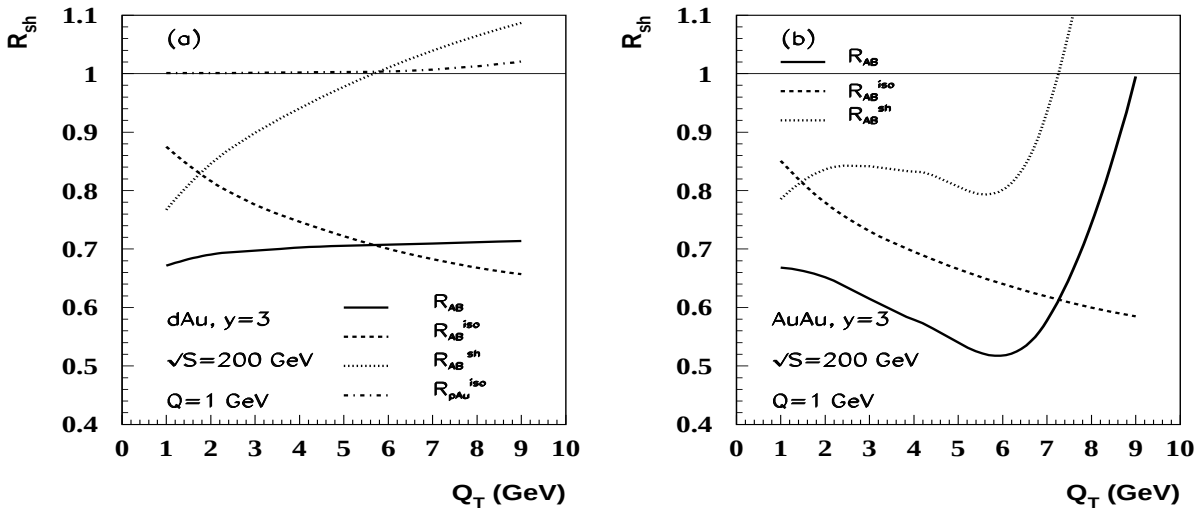

FIG. 15. The ratio R_{AB} at RHIC in the forward region ($y = 3$) for (a) dAu and (b) $AuAu$ collisions at Q =1 GeV as a function of Q_T.

Figure 16 shows R_{AB} as a function of Q_T at the LHC in pPb and $PbPb$ collisions at both, central rapidity and forward rapidity. In pPb collisions the Drell-Yan pair production is suppressed more in the forward region, as expected. However, it is surprising that in $PbPb$ collisions, the Drell-Yan pair production in the forward region is actually slightly less suppressed than in the central rapidity region, up to $Q_T \approx 13$ GeV. This behavior is very different from what was found at RHIC. It can be explained by the very different values of x_1 and x_2. From the central rapidity region to the forward rapidity region, x_1 increases and x_2 decreases. From Fig. 11, approximately, x_2 changes from on the order of 10^{-3} to on the order of 10^{-4} if one wants to produce a low-mass Drell-Yan pair not at $y = 0$ but at $y = 2.4$. At the same time, x_1 changes from on the order of 10^{-3} to on the order of 10^{-2}. In the EKS parameterization, the shadowing factors are almost constant in $[10^{-3}, 10^{-4}]$. However, shadowing effects decrease much in the region $[10^{-3}, 10^{-2}]$. This leads to the slight increase of Drell-Yan pair production in the forward region compared to the central rapidity region. Gluon saturation (color glass condensate) effects [20,25,26] may make the increase even larger.

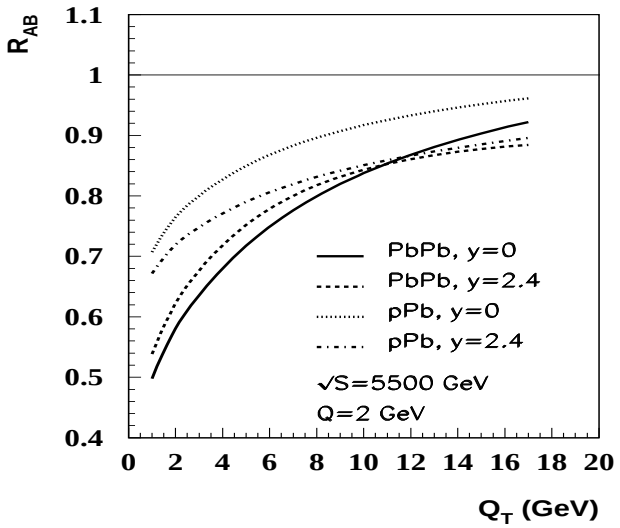

FIG. 16. The ratios R_{AB} at the LHC at Q =2 GeV for pPb at $y = 0$ (dotted), pPb at $y = 2.4$ (dash-dot), $PbPb$ at $y = 0$ (solid), and $PbPb$ at $y = 2.4$ (dashed) as a function of Q_T.

VII. SUMMARY AND CONCLUSION

In summary, low-mass Drell-Yan dilepton production is a potentially clean probe of small-x gluons, without strong final-state interactions. When $Q_T > 2$ GeV, the gluon initiated sub-processes contribute more than 80% to the cross section. Unfortunately, low-mass Drell-Yan dilepton production suffers from low production rate at RHIC due to the Drell-Yan factor. At the Tevatron and LHC energies, high-Q_T low-mass Drell-Yan production is an excellent probe of the gluon distributions.

We have shown that the production rate for low-mass Drell-Yan pairs at Tevatron and LHC energies does not reduce for a wide range of rapidity, and the forward region is very sensitive to small-x gluons. Therefore, the rapidity distribution of low-mass Drell-Yan pairs at large enough transverse momentum could be a good and clean probe of small-x gluons at collider energies.

Because of the lack of final-state interactions and the relatively weak initial-state nuclear-dependent power corrections at high Q_T, the rapidity and transverse momentum distribution of low-mass Drell-Yan pairs in hadron-nucleus and nucleus-nucleus collisions should be a very good probe of the gluon distribution in a nucleus. By comparing the nuclear modification factor of pAu and dAu, we demonstrated quantitatively that the isospin effect is very important in extracting nuclear parton distributions. We have shown that low-mass Drell-Yan pairs in the forward region at Tevatron and LHC energies provide very sensitive information on the gluon distribution and its nuclear dependence for x less than 10^{-4}. With such sensitivity on gluons, low mass Drell-Yan dilepton can be a good probe of the novel phenomena of gluon saturation or color glass condensate in a large nucleus. We believe that in view of the importance of small-x gluons, the ability of low-mass Drell-Yan pairs to provide information on these gluon distributions as demonstrated in the present paper warrants the mounting of experimental efforts to measure low-mass Drell-Yan pairs at colliders.

ACKNOWLEDGMENTS

We are grateful to Mike Albrow and Mark Strikman for discussions about small-x gluon physics at CDF. This work was supported in part by the U.S. Department of Energy, under grants DE-FG02-86ER40251 and DE-FG02-87ER40371.

REFERENCES

[1] J. Huston, S. Kuhlmann, H. L. Lai, F. I. Olness, J. F. Owens, D. E. Soper and W. K. Tung, Phys. Rev. D **58**, 114034 (1998) [arXiv:hep-ph/9801444].

[2] J. Pumplin, D. R. Stump, J. Huston, H. L. Lai, P. Nadolsky and W. K. Tung, JHEP **0207**, 012 (2002) [arXiv:hep-ph/0201195].

[3] A. D. Martin, R. G. Roberts, W. J. Stirling and R. S. Thorne, Eur. Phys. J. C **35**, 325 (2004) [arXiv:hep-ph/0308087].

[4] K. J. Eskola, H. Honkanen, V. J. Kolhinen, J. W. Qiu and C. A. Salgado, Nucl. Phys. B **660**, 211 (2003) [arXiv:hep-ph/0211239].

[5] J. W. Qiu, Nucl. Phys. B **291**, 746 (1987).

[6] L. L. Frankfurt, M. I. Strikman and S. Liuti, Phys. Rev. Lett. **65** (1990) 1725.

[7] K. J. Eskola, Nucl. Phys. B **400** (1993) 240.

[8] K. J. Eskola, V. J. Kolhinen and C. A. Salgado, Eur. Phys. J. C **9** (1999) 61 [arXiv:hep-ph/9807297].

[9] K. J. Eskola, V. J. Kolhinen and P. V. Ruuskanen, Nucl. Phys. B **535** (1998) 351 [arXiv:hep-ph/9802350].

[10] M. Hirai, S. Kumano and M. Miyama, Phys. Rev. D **64** (2001) 034003 [arXiv:hep-ph/0103208].

[11] Z. Huang, H. J. Lu and I. Sarcevic, Nucl. Phys. A **637** (1998) 79 [arXiv:hep-ph/9705250].

[12] S. y. Li and X. N. Wang, Phys. Lett. B **527** (2002) 85 [arXiv:nucl-th/0110075].

[13] L. Frankfurt, V. Guzey, M. McDermott and M. Strikman, JHEP **0202** (2002) 027 [arXiv:hep-ph/0201230].

[14] K. J. Eskola, H. Honkanen, V. J. Kolhinen and C. A. Salgado, Phys. Lett. B **532** (2002)

222 [arXiv:hep-ph/0201256].

[15] N. Armesto, Eur. Phys. J. C **26** (2002) 35 [arXiv:hep-ph/0206017].

[16] A. Accardi *et al.*, arXiv:hep-ph/0308248.

[17] E. L. Berger, L. E. Gordon and M. Klasen, Phys. Rev. D **58**, 074012 (1998) [arXiv:hep-ph/9803387].

[18] E. L. Berger and J. W. Qiu, Phys. Lett. B **248**, 371 (1990).

[19] E. L. Berger, J. W. Qiu and X. f. Zhang, Phys. Rev. D **65**, 034006 (2002) [arXiv:hep-ph/0107309].

[20] G. Fai, J. W. Qiu and X. f. Zhang, J. Phys. G **30**, S1037 (2004) [arXiv:hep-ph/0403126].

[21] J. W. Qiu and X. f. Zhang, Phys. Rev. D **64**, 074007 (2001) [arXiv:hep-ph/0101004].

[22] C. Albajar *et al.*, UA1 Collaboration, Phys. Lett. **B209**, 397 (1988).

[23] V. Guzey, M. Strikman and W. Vogelsang, arXiv:hep-ph/0407201.

[24] J. W. Qiu and X. f. Zhang, Phys. Lett. B **525**, 265 (2002) [arXiv:hep-ph/0109210].

[25] J. Jalilian-Marian, Nucl. Phys. A **739**, 319 (2004) [arXiv:nucl-th/0402014].

[26] R. Baier, A. H. Mueller and D. Schiff, Nucl. Phys. A **741**, 358 (2004) [arXiv:hep-ph/0403201].